



HAL
open science

Simultaneous observation of the anomerization and reaction rates of enzymatic dehydrogenation of glucose-6-phosphate by dissolution-DNP

Mehdi Soussi-Therond, David Guarin, Aiky Razanahoera, Yongmin Zhang, Mathieu Baudin, E Miclet, Nicolas Giraud, Daniel Abergel

► To cite this version:

Mehdi Soussi-Therond, David Guarin, Aiky Razanahoera, Yongmin Zhang, Mathieu Baudin, et al.. Simultaneous observation of the anomerization and reaction rates of enzymatic dehydrogenation of glucose-6-phosphate by dissolution-DNP. *Journal of the American Chemical Society*, 2024, 146 (50), pp.34651-34660. 10.1021/jacs.4c12904 . hal-04857648

HAL Id: hal-04857648

<https://hal.science/hal-04857648v1>

Submitted on 28 Dec 2024

HAL is a multi-disciplinary open access archive for the deposit and dissemination of scientific research documents, whether they are published or not. The documents may come from teaching and research institutions in France or abroad, or from public or private research centers.

L'archive ouverte pluridisciplinaire **HAL**, est destinée au dépôt et à la diffusion de documents scientifiques de niveau recherche, publiés ou non, émanant des établissements d'enseignement et de recherche français ou étrangers, des laboratoires publics ou privés.

Simultaneous observation of the anomerization and reaction rates of enzymatic dehydrogenation of glucose-6-phosphate by dissolution-DNP

Mehdi Soussi-Therond¹, David Guarin¹, Aiky Razanahoera¹, Yongmin Zhang^{2,3},
Mathieu Baudin^{1,4}, Emeric Miclet¹, Nicolas Giraud⁴, and Daniel Abergel ^{*1}

¹Laboratoire des biomolécules, LBM, Département de chimie, Ecole normale supérieure, PSL University, Sorbonne Université, CNRS, 75005 Paris, France.

²Sorbonne Université, CNRS, Institut Parisien de Chimie Moléculaire, UMR 8232, 4 Place Jussieu, 75005 Paris, France

³School of Pharmaceutical Sciences, Zhejiang Chinese Medical University, Hangzhou, Zhejiang 311422, China

⁴Laboratoire de Chimie et Biochimie Pharmacologiques et Toxicologiques, LCBPT UMR 8601, Université Paris Cité, 45, Rue des Saints Pères, 75006 Paris, France

December 26, 2024

Abstract

The hyperpolarization of biological samples using dissolution-dynamic nuclear polarization (dDNP) has become an attractive method for the monitoring of fast chemical and enzymatic reactions using NMR by taking advantage of large signal increase. This approach is actively developing, but still needs key methodological breakthroughs to be used as an analytical method for the monitoring of complex networks of simultaneous metabolic pathways. In this article, we use the deceptively simple example of glucose-6-phosphate (G6P) oxidation reaction by the enzyme G6P dehydrogenase (G6PDH) to discuss some important methodological aspects of dDNP kinetic experiments, such as its robustness and its ability to provide repeatable results, as well as the capacity of this time resolved methodology to test kinetic models and hypotheses, and to provide reliable parameter estimates. To illustrate the potential of our approach, we report the first direct and quantitative evidence of selectivity of G6PDH towards the β anomer of G6P.

1 Introduction

Nuclear magnetic resonance (NMR) spectroscopy has proven a unique approach to investigate the kinetics of chemical and enzyme reactions, by allowing simultaneous identification and monitoring of both their substrates and products. However, the low sensitivity of NMR often limits its application to reactions with slow time scales. This can be overcome using dissolution dynamic nuclear polarization (dDNP) techniques. Thus, by hyperpolarizing magnetically active nuclei at cryogenic temperatures, and by observing their signals in ambient conditions after transfer to a conventional spectrometer, spectra with a signal increase of 4-5 orders of magnitude can be obtained. Since the introduction of dDNP two decades ago,¹ a number of studies have demonstrated the potential of this technique to study dynamic processes *in vitro*,^{2;3} including enzymatic^{4;5;6;7;8} and chemical⁹

*daniel.abergel@ens.psl.eu

reactions involved in biological processes. Alternatively, a number of *in cell* dDNP experiments have also been proposed that provided insight on kinetic pathways in the cell.^{10;11;12}

The metabolism of glucose is one of the most fundamental cellular processes. Indeed, glucose is the primary substrate of glycolysis and of the pentose phosphate pathway (PPP), both known to involve complex and regulated networks of enzymatic reactions. Importantly, past studies tend to suggest that the two anomers of glucose are involved in different ways, glycolysis specifically targeting the α anomer of glucose,¹³ whereas only its β anomer enters the PPP.¹⁴ The anomer selectivity of these metabolic pathways is associated to enzymatic mutarotation of glucose^{15;16} and G6P^{17;18;19} in the cell, catalyzed by aldose-1-epimerases. These kinetics have been recently investigated by NMR for fluorinated²⁰ and phosphorylated²¹ hexoses.

Alternatively, both glucose and G6P undergo spontaneous mutarotation $\alpha \rightleftharpoons \beta$, a process that has been the subject of many studies.^{14;16;22} Spontaneous anomeric exchange for G6P, which is favored by the intramolecular acid base catalysis,²² takes place on a time scale that has been shown to be two orders of magnitude faster than for glucose.^{14;22} Thus, glucose has a typical exchange time on the order of tens of minutes, whereas for G6P, α/β equilibrium is reached on a time scale of the order of the minute.⁹ This has direct consequences for the kinetic study of fast enzymatic reactions performed in dDNP conditions, where the time windows of chemical reaction and mutarotation overlap with the observation window. Thus, in the case of glucose, spontaneous anomer exchange can be disregarded when studying the kinetics of reactions that are completed within a few tens of seconds, the typical observation duration of dDNP. In contrast, the much faster G6P mutarotation makes the catalytic dehydrogenation by glucose-6-phosphate dehydrogenase (G6PDH) more complex to analyze, as both processes cannot be observed separately. This is also the case for other enzymes targeting selectively one of the G6P anomers, such as the α -anomer specific G6P isomerase in yeast.¹⁴

DDNP investigations of fast enzyme reactions involving G6P as the substrate require to take both catalysis and anomer exchange into account, and to analyze them simultaneously. Such a combination of fast processes introduces further complexity, as we recently noticed in a previous dDNP study of enzymatic reactions and cascades thereof.⁹ Besides, a recent dDNP study of the G6P anomer exchange kinetics was conducted using the enzymatic phosphorylation of glucose by Hexokinase.²³

In this article, we present a kinetic study of the G6P oxidation by the enzyme G6P dehydrogenase (G6PDH), the first enzyme of the PPP that produces δ -phospho-gluconolactone,²⁴ using dDNP. We use this deceptively simple example to discuss some important methodological aspects of dDNP kinetic experiments *in vitro*, such as its robustness and its ability to provide repeatable results, as well as the capacity of this time resolved methodology to test kinetic models and hypotheses, and to provide reliable parameter estimates. Such aspects have apparently been somewhat neglected so far.

Materials and Methods

Production and purification of [U-¹³C; U-²H]G6P. Doubly labelled G6P was produced and purified using an *ad hoc* protocol developed in our laboratory²⁵ and optimized for this work. [U-¹³C, U-²H]-G6P was enzymatically produced in a reaction medium containing 1.4 mg of Hexokinase (Sigma Aldrich) from *Saccharomyces cerevisiae* (corresponding to 100 U), $2.6 \cdot 10^{-3}$ moles of [U-¹³C, U-²H]-Glucose (Sigma Aldrich), $3.4 \cdot 10^{-3}$ moles of ATP (Sigma Aldrich) in 45 mL of a 100 mM Phosphate Buffer (pH = 7.25) and $6.9 \cdot 10^{-2}$ M of MgCl₂ solution (Sigma Aldrich). The reaction was monitored by ³¹P and ¹³C NMR and completion attested after 25 h at ambient temperature. The reaction medium was then lyophilized, and the obtained solid was dissolved in the least possible H₂O volume. This solution was then purified by size-exclusion chromatography (SEC) on a Sephadex® G25 resin. Fractions of 3 mL containing carbohydrates were collected and identified by a dehydration reaction with sulfuric acid (Figure SI-5 in the SI). Fractions #40 to #60 containing carbohydrates (brown spots) were lyophilized, weighted (Table SI-3), and the solids obtained were dissolved in 500 μ L D₂O. The amounts of G6P in these samples were measured by means of ¹³C NMR. Peak assignment is presented in Fig. SI-7 of the Supplementary Information. For quantification purposes, a capillary containing a 60 mM solution of ¹³C-labelled glycine was placed

inside an NMR tube filled with these 500 μL volumes of resuspended fractions. Quantification was performed using $^{13}\text{C}_1$ (sum of both anomers) and $^{13}\text{C}_6$ resonance peaks. The $^{13}\text{C}_2 - ^{13}\text{C}_5$ region, was used for cross-checking (see Figure SI-8 in Supplementary Information).

Quantification of ADP and ATP. Quantification was performed using ^{31}P NMR by comparing the intensities of their respective peaks with that of the ^{31}P G6P resonance, the concentration of which was previously obtained by ^{13}C NMR. (see Figure SI-9 in the Supplementary Information). The results are displayed in Table SI-4 of the Supplementary Information, together with the results of the quantification of G6P. Sephadex G-25 is a well established gel filtration medium for desalting. We observed by ^{31}P NMR a total clearance of the phosphate buffer in the analysed fractions #44 to #47. However, due to the similar sizes of $[\text{U-}^{13}\text{C}, \text{U-}^2\text{H}]\text{-G6P}$, ADP and ATP ($[\text{U-}^{13}\text{C}, \text{U-}^2\text{H}]\text{-G6P}$: 279 Daltons, ADP: 427 Daltons, and ATP: 507 Daltons), these molecules were only partially separated. We found that fraction #45, although not the fraction containing the highest amount of G6P (see Figure SI-6 in the Supplementary Information), corresponded to the purest in terms of ATP and ADP contamination (90% purity).

DNP sample preparation. The hyperpolarized sample consisted of a 75- μL volume comprising 266 mM of $[\text{U-}^{13}\text{C}, \text{U-}^2\text{H}]\text{-G6P}$ (20 micromoles) in 10%:40%:50% (v:v:v) solution of $\text{H}_2\text{O}:\text{D}_2\text{O}:\text{Glycerol-d}_8$ with (4-hydroxy-2,2,6,6-tetramethylpiperidine-1-oxyl) as the polarizing agent, at a concentration of 40 mM. Once prepared, the sample was inserted into a Bruker prototype polarizer operating at 6.7 T and at a temperature of $T=1.2$ K.

Enzyme solution. The NMR tube contained 600 μL of a 0.1 M HEPES buffer at pH 7.4, 100 μL of D_2O , 50 μmol of MgCl_2 , 134 μmol of NADP^+ , for a total volume of 1 mL (cofactor in excess to ensure complete substrate conversion by the end of the experiment), as well as 120 μL of a 1 M NaOH solution (to fix the pH at 7.4). In addition, 150 μL of a ~ 1 U/ μL solution of G6PDH from *E. coli* (Nzytech) was added to the buffer in the NMR tube.

DNP hyperpolarization experiments. Experiments were performed on a 6.7 T Bruker prototype polarizer operated at 1.2 K. The μwave power was set to 350 mW and irradiation was performed at 187.9 GHz, modulated with a saw-tooth function over a range of 100 MHz. Polarization of ^{13}C nuclei was achieved using cross-polarization transfer from ^1H ²⁶ every 4 minutes. Monitoring of the evolution of the signal was achieved by small-angle ^{13}C read pulses (10°) until a maximum ^{13}C polarization has been reached. Maximum polarization was typically reached after ~ 6 CP steps (\sim one hour) under $\mu\text{-wave}$ irradiation. Dissolution was then performed with 4.5 mL of 0.1 M HEPES buffer at pH 7.4 and 0.5 mL of D_2O , heated to 150°C and at 11 bar pressure, that was flushed onto the frozen, hyperpolarized, sample. The liquid was then transferred under a continuous flow of pressurized Helium gas into a 10 mm NMR tube sitting inside a 9.4 T wide-bore NMR spectrometer. In order to avoid spurious delays during transfer, the polarized solution was directly pushed through a teflon tubing of 1.6 ID to the NMR tube in the NMR spectrometer located ~ 7 m away from the polarizer, under Helium gas pressure (8 bars) for 3 seconds, after which acquisition started. The volume of hyperpolarized solution reaching the NMR tube was 3 mL so that the final sample volume was ~ 4 mL. Filling of the NMR tube was complete after ~ 4 s. In the current system, in order to increase the speed of transfer and minimize the polarization losses during transfer, no phase separator was used, so that the droplets of the hyperpolarized solution were not thermalized by way of a heat exchanger, as in other setups.^{27;28} The liquid reaching the NMR tube then mixed with the enzyme solution that kept at the regulated temperature in the spectrometer (27°C).

NMR experiments Experiments were acquired on a 9.4 T (400 MHz) Bruker spectrometer equipped with a 10 mm BBO dual channel probe. Enzymatic reactions were monitored by ^{13}C NMR experiments where both ^1H and ^2H decoupling were performed using a Waltz-16 sequence²⁹ during acquisition. Spectra were acquired using 10° excitation pulses. Acquisition time was 300 ms and the delay between scans was 1 s. In these experiments, the carrier was set to 115 ppm, close to the resonance frequencies of the α and β anomer ^{13}C signals (respectively at 91.5 ppm and

95.3 ppm), and the spectral width was 22.05 kHz (220 ppm). All experiments were performed at 27°C. The recording of the spectra by the NMR spectrometer is triggered by dissolution, so that the first few spectra monitor the filling of the NMR tube with the hyperpolarized solution (see above). Complete filling of the NMR tube was attested by the decay of the hyperpolarized glycerol signal, not involved in the reaction, and only subsequent data points, i.e., ~ 7 s from dissolution, were used for the kinetic analysis. This defined the initial time t_0 of the kinetic sampling.

Data processing and analysis Data were processed using the TOPSPIN $\text{\textcircled{R}}$ software. Zero-filling was applied to extend the ^{13}C free induction decay (FID) signals from 16k to 32k points prior to the Fourier transform. An exponential apodization window (10 Hz line broadening) was used and spectra were baseline corrected. Resonance signals were fitted by Lorentzian functions as in previous work,⁸ using the Broyden–Fletcher–Goldfarb–Shanno (BFGS) algorithm³⁰ as implemented in the optim command of the Scilab software³¹. Peak intensities were computed by numerical integration of these Lorentzian lines. DDNP buildup and decay curves were fitted to the kinetic model using the Differential Evolution algorithm,³² implemented in a homemade Scilab routine. This is a genetic kind of algorithm that searches iteratively for improved sets of candidate solutions, based on a guided random search of new parameters. In contrast to gradient-based methods, it does not require differentiation and is therefore fast and avoids the program to be trapped in local minima and, when converged, ensures convergence to the global minimum (for general references, see ref.^{33;34}). At each step of the minimization process, computation of the test solution of the linear differential system of Eq. 2, of the form $\frac{d}{dt}\mathbf{X} = \mathbf{A}\mathbf{X}$, was performed using the eigenvalue representation: $\mathbf{X}(t) = \mathbf{U}e^{\mathbf{A}(t-t_0)}\mathbf{U}^{-1}\mathbf{X}(t_0)$, where $\mathbf{A} = \mathbf{U}\mathbf{\Lambda}\mathbf{U}^{-1}$. This avoided numerical integration of the differential system at each step of the parameter search. The net loss of magnetization at the n^{th} time point of the kinetics sampled every Δt , and due to the $\theta = 10^\circ$ read pulse, was taken into account for the analysis of the signal $\mathbf{S}(t)$:

$$\mathbf{S}(t) = \mathbf{U}e^{\mathbf{A}n\Delta t}\mathbf{U}^{-1}\mathbf{S}(t_0) \quad (1)$$

2 Results and Discussion

To monitor G6P oxidation by G6PDH, we hyperpolarized a G6P sample following the protocol described above, and recorded a series of ^{13}C NMR spectra after its transfer into an NMR tube containing the enzyme. Experiments were performed with 150 units of enzyme activity (determined according to the supplier - Nzytech, 5000 U in 5 mL suspension). In our experiments, the initial concentration ratio in the NMR tube of NADP^+ over $[\text{U-}^{13}\text{C}, \text{U-}^2\text{H}]\text{-G6P}$ was ~ 6.7 . The variation of $[\text{NADP}^+]$ during the course of the experiment was therefore neglected, and was assumed approximately constant during the reaction. Experiments were acquired with proton and deuterium decoupling, and only the $^1\text{J}_{\text{C-C}}$ couplings of ^{13}C are resolved, leading to the hyperpolarized ^{13}C spectrum obtained after dissolution shown in Figure 1. The ^{13}C resonance lines of the α and β anomer are located at 91.5 and 95.3 ppm, and the resonance peak at 174 ppm attests for the presence of the δ -PGL carbonyl ^{13}C . The oxidation reaction was thus monitored through the respective decay and buildups curves of the anomeric and carbonyl peak intensities. The typical reaction kinetic profiles, as depicted in Figure 1, were fitted to the model of Eq. 2 shown below.

The kinetic curves of the three compounds were analyzed assuming first-order kinetics for all the reactions involved in the reaction pathway, which comprises mutarotation between the α and β anomers of G6P, and their oxidation by the G6PDH enzyme. As mentioned above, both processes take place on overlapping time scales on the order of a few tens of seconds. The enzyme reaction requires NADP^+ as a cofactor, which was added in large excess with respect to G6P (~ 6.7 fold) to the solution so that oxidation was considered a pseudo-first order kinetics. Moreover, the kinetic model of the reaction pathway was further simplified by assuming that the isomerisation of the reaction product, δ -PGL, into γ -PGL, and the hydrolysis of both into 6-phosphogluconic acid (6PGA)^{9;24} could be accounted for by a simple exponential leakage, i.e., a first order rate process. This reaction pathway is summarized in the scheme of Figure 2, and leads to the kinetic model for

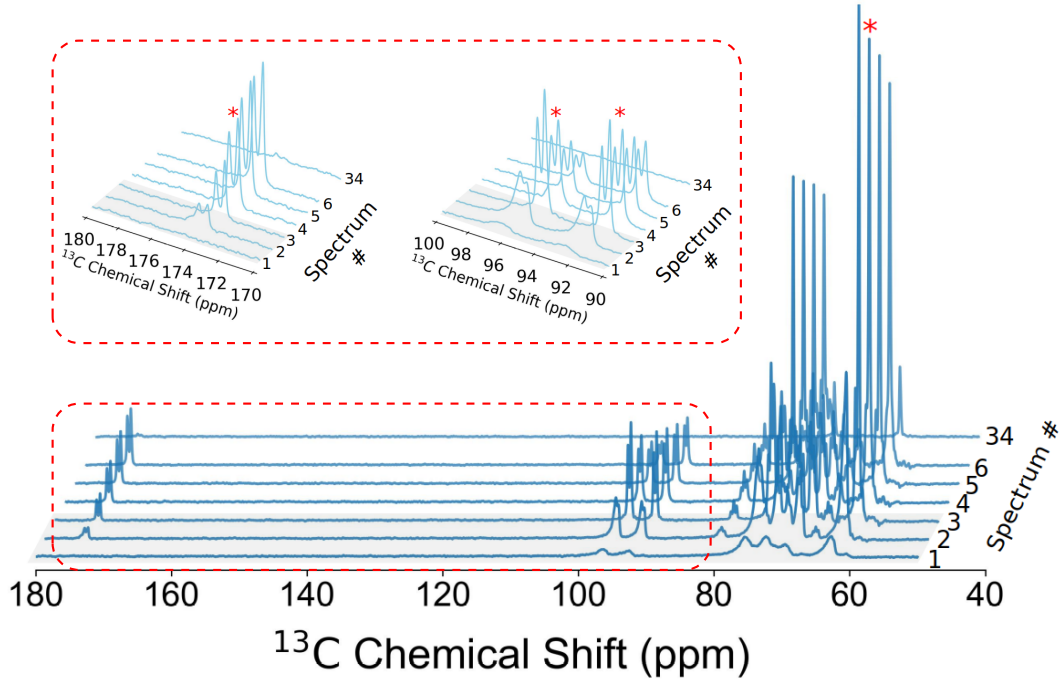


Figure 1: The ^{13}C NMR spectrum of the sample is shown together with the buildup and decay curves of δ -PGL, α -G6P and β -G6P NMR signal intensities. The insets show the stack plot of the lactone buildup and of the anomeric peaks of the G6P under enzymatic oxidation of G6P. The spectra acquired at early times after dissolution, during the filling of the NMR tube with the hyperpolarized solution (shaded area), are discarded for the kinetic analysis. Complete filling is attested by the decay of the glycerol-d8 signal (rightmost peak) that does not take part in the reactions. The first spectrum used for the kinetic analysis is marked by a star.

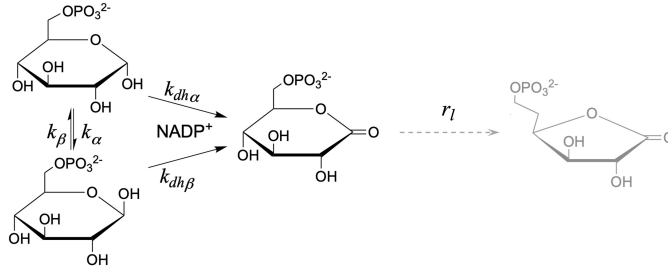


Figure 2: Simplified reaction pathway of G6P dehydrogenation by G6PDH. $k_{\alpha,\beta}$ are the α/β anomer exchange rate constants; $k_{dh\alpha,\beta}$ denote the enzyme reaction rates for each anomer.

the magnetizations of α and β G6P anomers and the lactone, resp. $m_{z\alpha}$, $m_{z\beta}$, m_{zl} , given by Eqs. 2:

$$\frac{d}{dt} \begin{pmatrix} m_{z\alpha} \\ m_{z\beta} \\ m_{zl} \end{pmatrix} = \begin{pmatrix} -r_\alpha - k_\alpha - k_{dh\alpha} & k_\beta & 0 \\ k_\alpha & -r_\beta - k_\beta - k_{dh\beta} & 0 \\ k_{dh\alpha} & k_{dh\beta} & -r_l \end{pmatrix} \begin{pmatrix} m_{z\alpha} \\ m_{z\beta} \\ m_{zl} \end{pmatrix} \quad (2)$$

where r_α , r_β are the longitudinal relaxation rates of the α and β ^{13}C anomers; k_α , k_β are the anomer exchange rates; $k_{dh\alpha}$ and $k_{dh\beta}$ are the enzyme reaction rates for both G6P anomers, and r_l is an empirical "leakage" rate constant that takes into account the ^{13}C carbonyl relaxation rate of the δ -PGL as well as the isomerisation with γ -PGL and their degradation into 6-phosphogluconic acid (6PGA).^{9;24}

With the aim of retrieving quantitative kinetic parameters from dDNP experiments, it is important to assess the robustness of the experimental setup, which implies that repeated experiments

are equally well fitted with the same sets of parameters. Therefore, and in order to test the robustness of the experimental protocol, the experiment was performed in triplicate. This question is most naturally addressed by the study of the eigenmodes and eigenvectors that fully characterize the evolution of the differential system Eqs.2. Because the relations between the eigenvalues and the kinetic parameters are not one-to-one, they provide a more convenient quantity that we present prior to the analysis of chemically relevant parameters. Since the decay rate constant r_l is an obvious root of the characteristic equation:

$$(r_l + \lambda) [(r_\alpha + k_\alpha + k_{dh\alpha} - \lambda)(r_\beta + k_\beta + k_{dh\beta} - \lambda) - k_\alpha k_\beta] = 0, \quad (3)$$

the eigenvalues are simply given by:

$$\begin{aligned} \lambda_1 &= -\frac{1}{2}(k_\alpha + k_\beta + k_{dh\alpha} + k_{dh\beta} + r_\alpha + r_\beta + \sqrt{\Delta}) \\ \lambda_2 &= -\frac{1}{2}(k_\alpha + k_\beta + k_{dh\alpha} + k_{dh\beta} + r_\alpha + r_\beta - \sqrt{\Delta}) \\ \lambda_3 &= -r_l \end{aligned} \quad (4)$$

with $\Delta = (r_\alpha + k_\alpha + k_{dh\alpha} + r_\beta + k_\beta + k_{dh\beta})^2 - 4k_\alpha k_\beta$. The model provided perfect fitting of the different experiments with the data (see Figure 3).

Since the main source of experimental error in the NMR signal is caused by random fluctuations in the receiver circuit during acquisition, this detector-limited noise process is customarily modeled by a Gaussian white noise (see for instance references^{35;36}). Therefore, error estimation of the experimental intensities was performed in a straightforward manner by way of the well-established Monte Carlo method,³⁰ assuming a Gaussian distribution $\mathcal{N}(0, \sigma)$, where σ the experimental root mean square deviation of the NMR noise. The resulting error bars are indicated in Figure 3. Of course, the same Monte Carlo analysis also provides error estimates of the relevant model parameters. However, in a first round of evaluation, we focused on the eigenvalues of Eqs. 4, and the same analysis was performed for each experiment separately. The three separate probability distributions, obtained by the above mentioned Monte Carlo simulations, are depicted in Figure 4, and the associated values of their averages and standard deviations are reported in Table 1. It is noteworthy that the eigenvalue distributions in Figure 4 are well fitted by a Gaussian functions and that all eigenvalues show satisfactory dispersions, as can be seen from Table 1. Note that experiment #2 is associated to a broader distribution of the eigenvalues, which can be ascribed to the lower signal to noise ratio, a consequence of the lower polarization achieved in the solid before dissolution.

	No constraint	$k_\alpha/k_\beta = 1.6 \pm 0.2$	$k_\alpha/k_\beta = 1.6 \pm 0.2$ and $r_\alpha = r_\beta$
Expt #1			
λ_1	-0.22 ± 0.01	-0.21 ± 0.01	-0.21 ± 0.01
λ_2	-0.48 ± 0.05	-0.48 ± 0.05	-0.46 ± 0.03
λ_3	-0.13 ± 0.01	-0.12 ± 0.01	-0.123 ± 0.004
Expt #2			
λ_1	-0.26 ± 0.04	-0.22 ± 0.02	-0.23 ± 0.02
λ_2	-0.48 ± 0.05	-0.58 ± 0.16	-0.56 ± 0.07
λ_3	-0.15 ± 0.03	-0.15 ± 0.03	-0.14 ± 0.02
Expt #3			
λ_1	-0.20 ± 0.01	-0.187 ± 0.003	-0.21 ± 0.01
λ_2	-0.55 ± 0.04	-0.40 ± 0.01	-0.52 ± 0.02
λ_3	-0.12 ± 0.01	-0.11 ± 0.01	-0.109 ± 0.003

Table 1: Eigenvalues obtained for 3 different experiments (150 U and 27°C). Values are expressed in s^{-1} units.

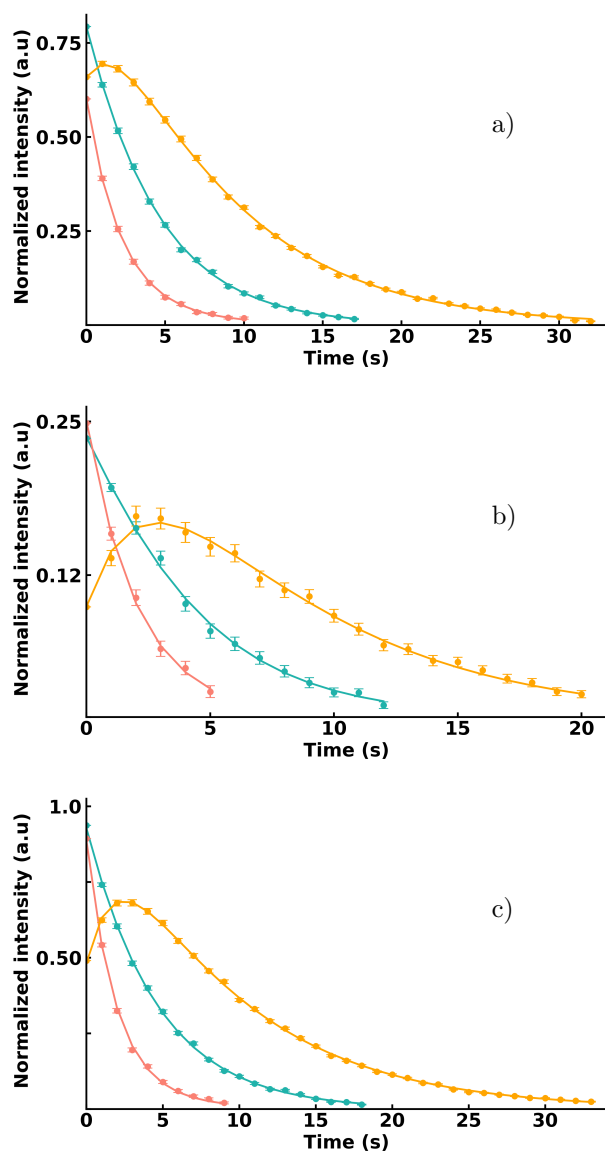


Figure 3: The time evolution of the ^{13}C NMR signals of three experiments are shown together with the best fits corresponding to the model shown in Equation 2. a), b) and c) correspond to 3 different acquisitions of the triplicate experiment. Solid lines indicate fits to the model of Equation (1). α -G6P, β -G6P and lactone intensities are depicted in blue, red and yellow, respectively. Error bars were obtained by a Monte Carlo simulations in each experiment (see text for details) The time axis is labelled from $t_0 = 0$ s, which corresponds to the first point of the kinetics analysis after complete filling the NMR tube, and decay of the glycerol signal (see *Material and Methods*) .

Assessing the repeatability of the experiment, that is, the robustness of the experimental setup as its ability to yield identical results, therefore identical model parameters, is the next purpose of this study. In this respect, the agreement between experiments, or discrepancies thereof, is best reflected by comparing the eigenvalues of the kinetic model (Eq. 2) obtained in each realization of the experiment. The differences between the eigenvalues extracted from different experiments may be related to a number of experimental features (mixing between hyperpolarized and enzyme solutions in the NMR tube, temperature changes during experiments, ...), that may be negligible but possibly affect the robustness of the method and are difficult to model. It would be desirable to make use of the standard statistical tools to estimate experimental uncertainties originating from these possible additional sources of error. Nevertheless, any statistical approach would require

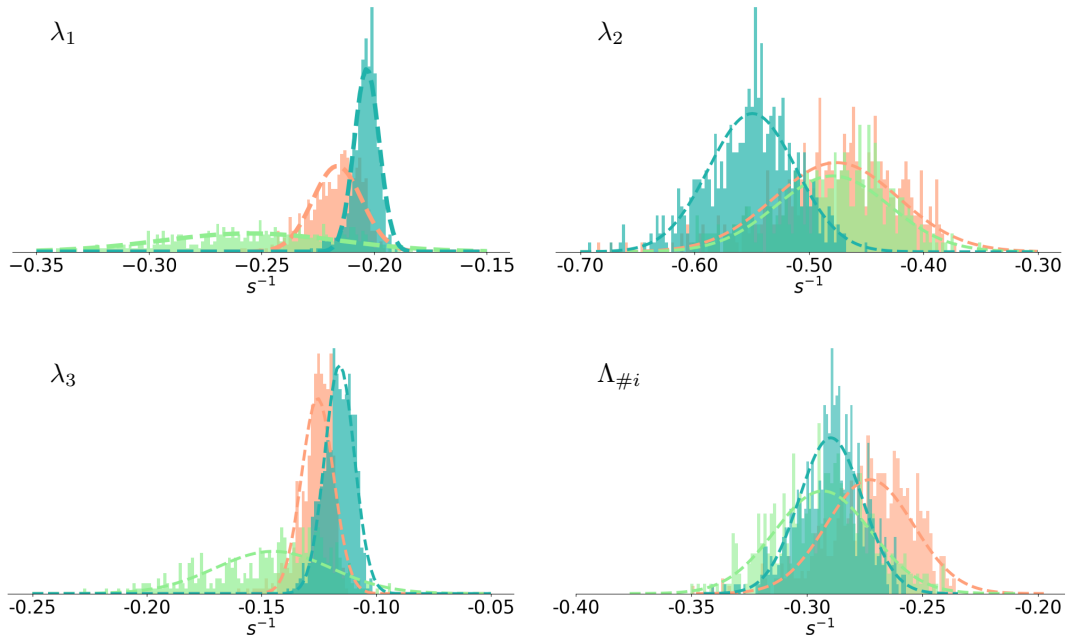


Figure 4: Model eigenvalues (Eqs. 4) extracted from three independent experiments. The distributions are obtained from 500 Monte Carlo simulations. The histograms depicted in orange, light green and blue, and corresponding to the first, second and third experiments, respectively, are given in Table 1. The histograms and Gaussian fits of the traces $\Lambda_{\#i}$, $i = 1, \dots, 3$ of the evolution matrix of Eq. 2 computed from each experiment of Figure 3 are displayed in the bottom right panel of the figure.

at least some knowledge about the “underlying process” leading to potential fluctuations of the measurements. This is the case for the Monte Carlo approach used in this study, or for any other approach such as a Markov chain Monte Carlo, which would require a knowledge of the support, i.e., the range of values of the measurement fluctuations, to ensure a minimum efficiency.³⁷ Inferring the values of such quantities would require to perform a large enough number of experiments to get any level of statistical significance, which is clearly out of reach in the present work.

In the absence of a statistically sound strategy, and in an attempt to estimate a global “error” from our set of three experiments, we *assumed* that computing the average and the standard deviation of the extracted model parameters would nevertheless provide some insight as to these unknown underlying process and serve as a basis for parameter error estimation.

Thus, the trace Λ_i of the kinetic matrix of Eq. 2 obtained from the Monte Carlo simulations was performed on each realization i of the triplicate experiment. This analysis yielded $\Lambda_{\#1} = -0.27 \pm 0.02 \text{ s}^{-1}$, $\Lambda_{\#2} = -0.31 \pm 0.04 \text{ s}^{-1}$, and $\Lambda_{\#3} = -0.29 \pm 0.01 \text{ s}^{-1}$, respectively. The associated distributions, depicted in Figure 4, show satisfactory agreement. Alternatively, the average and standard deviations of the merged eigenvalue distributions $\lambda_1, \lambda_2, \lambda_3$ of for the three experiments (see Figure 4 and Table 1) yielded the values $\lambda_1 = -0.22 \pm 0.02 \text{ s}^{-1}$, $\lambda_2 = -0.50 \pm 0.05 \text{ s}^{-1}$, $\lambda_3 = -0.13 \pm 0.02 \text{ s}^{-1}$. Overall, a plausible $\sim 10 - 15\%$ error on the eigenvalues could be estimated from these experiments.

2.1 Parameter estimation and prior information

The above analysis shows that the experimental data can be well fitted by a simple, first order kinetic model, with reasonable consistency between experiments. Now, the goal of this study, beyond the mere determination of eigenmodes, is to actually extract the values of the kinetic model parameters that describe the full reaction pathway under study. This task is rendered difficult because the complexity of the reaction network entails eigenmodes that are involved algebraic functions of the kinetic and relaxation parameters (see Eq. 4). Therefore, the relation between the extracted eigenmodes that characterize the kinetics during an experiment and the model parameters

are not one to one, and fitting may often lead to values that do not make physical sense. The presence of such meaningless parameter values was particularly marked for the anomer exchange rates k_α and k_β , which converged to values that did not agree with the expected ratio k_α/k_β obtained from the measured intensities of the β and α $^{13}\text{C}_1$ resonance lines at thermal equilibrium. Moreover, Monte Carlo simulations often showed broad distributions of the parameter values, as well as strong correlations between them. This is illustrated in Figure SI-3 of the Supplementary Information.

In order to overcome these difficulties and to improve parameter fitting, where we have introduced some prior knowledge. A readily available piece of information is the ratio $k_\alpha/k_\beta = 1.6 \pm 0.2$ of the mutarotation exchange rates, determined experimentally on a G6P sample at thermal equilibrium from the intensity ratio of the β over α $^{13}\text{C}_1$ anomeric signals. In this case, the relaxation rate distributions for both anomeric $^{13}\text{C}_1$, r_α and r_β , were not significantly different from each other in each experiment, on the basis of our Monte Carlo analysis (see Table SI-1). This conclusion is further supported by experiments reported in ref.²³ where indeed the authors found equal longitudinal relaxation times for ^{13}C in $[\text{U-}^{13}\text{C}, \text{U-}^2\text{H}]\text{-G6P}$ in dDNP experiments. Therefore, because prior knowledge of the ratio k_α/k_β did not sufficiently constrain all the remaining model parameters, these findings led us to introduce the further hypothesis that both anomers have identical relaxation rates. Results of the parameter fitting for the three experiments obtained with the prior constraints $r_\alpha = r_\beta$ and on k_α/k_β are summarized in Table 2 and Figure 5.

With this data analysis, our experiments led to significant observations. Interestingly, it was found that $k_{dh\beta} \approx 0.31 \pm 0.03 \text{ s}^{-1}$. Moreover, the value of $k_{dh\alpha}$ was essentially zero in all experiments.

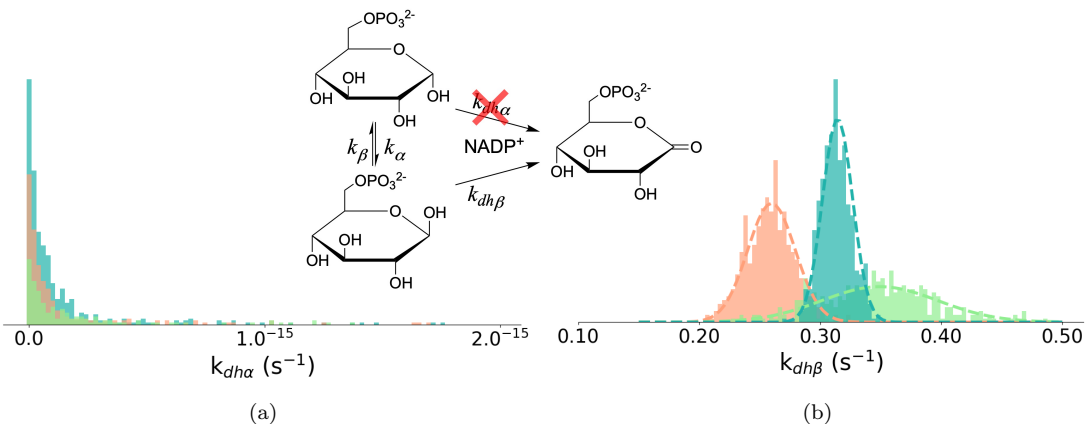


Figure 5: Parameter distributions of the $k_{dh\alpha}$, $k_{dh\beta}$ for the three experiments presented in this work. Dashed lines represent the Gaussian fits of the distributions with the experimental means and standard deviations.

Thus, the direct and quantitative estimate of this feature provided by the present study confirms previous observations from dDNP experiments.⁹ Interestingly enough, the values of the enzyme kinetic rate constant $k_{dh\beta}$ extracted from our experiments were actually robust and were rather insensitive to the use of prior information (see Tables 2 and SI-1), somewhat in contrast to other model parameters. Moreover, the kinetic rate constant values $k_{dh\alpha}$ and $k_{dh\beta}$ obtained by fitting the different realizations of the experiment agree reasonably well, as indicated in Table 2, which thus shows their robustness against experimental errors. Note that simultaneous fitting of the experiments lead to similar conclusions, which is illustrated in the histograms obtained from Monte Carlo simulations and depicted in Figs. SI-1 and SI-2, and in Table SI-2 in the SI.

In contrast, the analysis of $k_{dh\alpha}$ was found to be essentially zero in all experiments, thereby providing direct evidence of the substrate selectivity of G6PDH towards the β anomer of G6P. Such a substrate selectivity was already pointed out in ref.¹⁴. However, that study used glucose as a surrogate for G6P, and despite a ~ 200 -fold decrease of its overall activity, the enzyme was shown to have a selective action towards the glucose beta anomer. To our knowledge, the conclusion that $k_{dh\alpha} = 0$ of Salas *et al.*¹⁴ laid the basis for all subsequent models of G6P kinetic analyses,

typically measured using the coupled Hexokinase-G6PDH enzymes and using glucose as a primary substrate (see for instance refs. [18;19](#)). Here, in contrast, our experiments provide a direct estimate of $k_{dh\alpha} \approx 0$, to within experimental accuracy, and therefore fully justify the well accepted assumption of complete selectivity of G6PDH towards the β anomer of G6P.

The anomer exchange rates k_α and k_β are the other main kinetic parameters involved in the reaction pathway under study. These were also accessed by our experimental protocol that allowed us to obtain estimates of k_α and k_β . We thus obtained $k_\alpha = 0.042 \pm 0.017 \text{ s}^{-1}$ and $k_\beta = 0.029 \pm 0.012 \text{ s}^{-1}$, and their distributions are depicted in Figure [6\(a\)](#). These are in good agreement with the values given in ref. [19](#), $k_\alpha = 0.0658 \pm 0.0116 \text{ s}^{-1}$ and $k_\beta = 0.0389 \pm 0.0259 \text{ s}^{-1}$, that were obtained at 298 K based on conventional biochemical methods using UV spectroscopy.

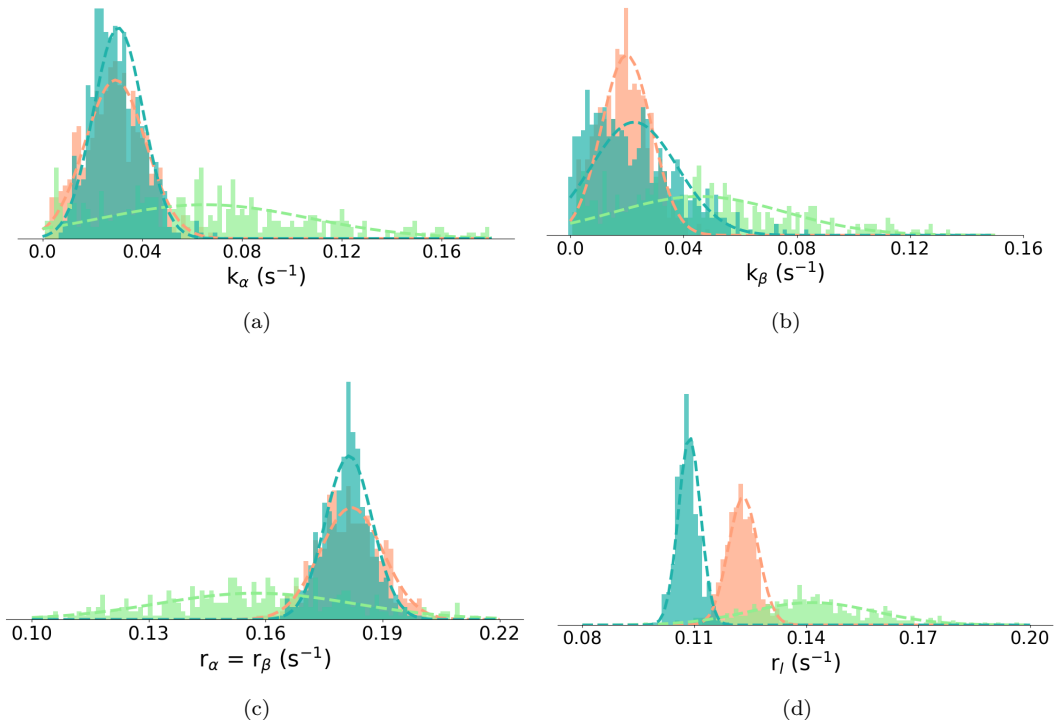


Figure 6: Parameter distributions of the k_α , k_β mutarotation rates, and $r_\alpha = r_\beta$, r_l relaxation rates for the three experiments presented in this work. Dashed lines represent the Gaussian fits of the distributions with the experimental means and standard deviations.

Besides, note that the values obtained in our work are somewhat lower than those of ref. [23](#), obtained through dDNP experiments performed at a higher temperature (313 K), and for which no error estimation was provided. We also note that the distributions of the experimental values of r_α ($= r_\beta$) obtained by Monte Carlo simulations for the different experiments overlap significantly, $r_{\alpha,\beta,1} \approx 0.18 \text{ s}^{-1}$, $r_{\alpha,\beta,2} \approx 0.16 \text{ s}^{-1}$, and $r_{\alpha,\beta,3} \approx 0.18 \text{ s}^{-1}$ (see Figure [6\(c\)](#)), which illustrates the robustness of our experimental protocol with respect to the relaxation parameter.

The sensitivity of this experimental protocol to experimental fluctuations, allowed us to assess the repeatability of the experimental dDNP setup and its limitations. The signal enhancement can potentially vary slightly because of altered polarization level achieved in the solid, due to partial crystallization of the DNP solution upon freezing, to variable amounts of substrate transferred to the spectrometer after dissolution. This transfer efficiency can vary between samples due to pressure or temperature variations of the solvent in the dissolution box, or to the human-dependent dissolution process. These technical problems essentially cause lower SNR in the kinetic experiments and larger parameter uncertainties but are not expected to alter the kinetic curves. The issue of mixing is somewhat different in this respect, as it may alter the buildup and decay curves of the observed species, which may be more deleterious for obtaining reliable kinetic parameters in these experiments. This limited robustness impacting the early stage of the experiment was

avoided by discarding early points, as detailed above, but nevertheless calls for instrumentation improvements and is the subject of ongoing work.^{38;39}

$k_\alpha/k_\beta = 1.6 \pm 0.2$ and $r_\alpha = r_\beta$	
Expt #1	
k_α	0.029 ± 0.010
k_β	0.020 ± 0.010
kdh_α	N.A
kdh_β	0.260 ± 0.020
r_α	0.180 ± 0.010
r_β	0.180 ± 0.010
r_l	0.123 ± 0.004
Expt #2	
k_α	0.065 ± 0.041
k_β	0.046 ± 0.030
kdh_α	N.A
kdh_β	0.350 ± 0.050
r_α	0.160 ± 0.030
r_β	0.160 ± 0.030
r_l	0.140 ± 0.020
Expt #3	
k_α	0.030 ± 0.010
k_β	0.023 ± 0.015
kdh_α	N.A
kdh_β	0.310 ± 0.010
r_α	0.180 ± 0.010
r_β	0.180 ± 0.010
r_l	0.109 ± 0.003

Table 2: Kinetic and relaxation parameters (in s^{-1}) obtained from three different dDNP experiments. Results were obtained with the use of prior knowledge of $k_\alpha/k_\beta = 1.6 \pm 0.2$ and with the assumption that $r_\alpha = r_\beta$.

Conclusions

Dissolution DNP has proven a useful tool to study fast, kinetic reactions in real time. Thus, in this work, we provide the first direct *and* quantitative evidence of selectivity of *E. coli* G6PDH towards the β anomer of G6P. Moreover, we have shown that it can be quite robust and provides satisfactorily repeatable results. In this regard, only a few time-resolved studies of chemical or enzymatic reactions by dDNP provide estimates of the experimental errors on kinetic parameters. In ref⁴⁰, Lee *et al.* extracted a pseudo-first order kinetic constant of the anionic polymerization of styrene based on three different measurements, and found errors comparable to ours. However, to our knowledge, no estimate of the error on the kinetic parameters that specifically relate to the repeatability of dDNP kinetic experiments are provided in the literature, in the context of enzymatic reactions *in vitro*.

Besides, analyzing complex reaction pathways remains a challenge, mainly because the kinetic and relaxation parameters that enter the model are entangled, which translates into strongly

correlated values in Monte Carlo simulations. As explained above, this requires independent experiments, and/or assumptions that allow to solve this undetermined problem.

The kinetic data were interpreted in terms of simple first order kinetics for both the anomer exchange and enzymatic reaction. The relevance of such an approach for an enzymatic reaction is questionable, as it is typically described by a Michaelis-Menten reaction scheme, possibly complexified by the presence of a cofactor, as in the present case⁴¹ or of an inhibitor⁴². It is well established that, in general, an order of reaction cannot be defined, and that enzymes obey a well-defined order kinetics to a good approximation only in some particular conditions.⁴² An account in the context of dDNP has been given recently.⁴³ Namely, in case of large substrate excess, the kinetics is approximately of zero order, meaning that the kinetic rate is constant with time. In this respect, it is interesting to note that, for comparable substrate polarization in the solid (to within $\sim 20\%$), roughly 80% of G6P has been transformed by the enzyme at the time of the first measurement after dissolution (see Fig. SI-4 in the Supplementary Information). This is a clear indication that the (fast) reaction has already significantly advanced before the start of acquisition, and the G6P concentration at the time of the first detected experiment is in the $\sim 400 \mu\text{M}$ range. Moreover, as mentioned above, the first 3-4 measurements - depending on which experiment - were actually discarded from the kinetic analysis to ensure that the filling of the MNR tube was complete. This means that the G6P concentration is also significantly smaller. The enzyme G6PDH has a putative bi bi random mechanism,^{41;44} for which values of the dissociation constants $K_{m,\text{G6P}}$ and K_{m,NADP^+} , with the enzyme and with the complexes $K_{m,\text{E-g6p}}$ and $K_{m,\text{E-NADP}^+}$ for *E. coli*^{44;45} are all in the $\sim 5 - 500 \mu\text{M}$ range.⁴⁶ In the conditions of our experiments, $[\text{NADP}^+]$ is always in excess (initially 35 mM upon mixing), so that the “effective” Michaelis K' constant for the (G6PDH/NADP⁺/G6P) complex is also expected to be in this range. From the above, this effective K'_m is likely of the same order as, or smaller than, $[\text{G6P}]$ at the time of measurements. The assumption of a zero order kinetic regime that may prevail at the early stage of the reaction was therefore unlikely.

Alternatively, the Michaelis-Menten approximately obeys a first order kinetics for low substrate concentrations. Surprisingly enough, and despite the fact that this condition may not be expected in the conditions of our experiments, our data are well fitted by a network of first order reactions only, including both the anomer exchange and enzymatic oxidation, in all the realizations of our kinetic experiment. One can therefore conclude that the results obtained with our experimental protocol and sample preparation empirically support a pseudo-first order enzyme kinetics, where the catalytic constant is given by the kinetic rate constant $k_{dh\beta}$. Further investigations are underway to shed more light on these aspects.

Supplementary Information Additional fitting results of kinetic parameters under various constraints, correlation plots of model parameters; comparison of the polarization levels obtained in the DNP experiments; experimental details of G6P purification and quantification (colorimetric tests and ¹³C and ³¹P NMR spectra).

References

- [1] Jan H. Ardenkjaer-Larsen, Björn Fridlund, Andreas Gram, Georg Hansson, Lennart Hansson, Mathilde H. Lerche, Rolf Servin, Mikkel Thaning, and Klaes Golman. Increase in signal-to-noise ratio of $> 10,000$ times in liquid-state nmr. *Proceedings of the National Academy of Sciences*, 100:10158–10163, 2003.
- [2] Mukundan Ragavan, Luigi I. Iconaru, Cheon-Gil Park, Richard W. Kriwacki, and Christian Hilty. Real-Time Analysis of Folding upon Binding of a Disordered Protein by Using Dissolution DNP NMR Spectroscopy. *Angewandte Chemie International Edition*, 56(25):7070–7073, JUN 12 2017.
- [3] Yaewon Kim, Mengxiao Liu, and Christian Hilty. Determination of binding affinities using hyperpolarized NMR with simultaneous 4-channel detection. *Journal of Magnetic Resonance*, 295:80–86, OCT 2018.

- [4] Adam W. Barb, S.K. Hekmatyar, John N. Glushka, and James H. Prestegard. Probing alanine transaminase catalysis with hyperpolarized ^{13}C -pyruvate. *Journal of Magnetic Resonance*, 228:59–65, 2013.
- [5] Hyla Allouche-Arnon, Ayelet Gamliel, Claudia M. Barzilay, Ruppen Nalbandian, J. Moshe Gomori, Magnus Karlsson, Mathilde H. Lerche, and Rachel Katz-Brull. A hyperpolarized choline molecular probe for monitoring acetylcholine synthesis. *Contrast Media and Molecular Imaging*, 6:139–147, 2011.
- [6] Hyla Allouche-Arnon, Ayelet Gamliel, Jacob Sosna, J. Moshe Gomori, and Rachel Katz-Brull. In vitro visualization of betaine aldehyde synthesis and oxidation using hyperpolarized magnetic resonance spectroscopy. *Chemical Communications*, 49:7076–7078, 2013.
- [7] Hyla Allouche-Arnon, Yonatan Hovav, Lanette Friesen-Waldner, Jacob Sosna, J. Moshe Gomori, Shimon Vega, and Rachel Katz-Brull. Quantification of rate constants for successive enzymatic reactions with dnp hyperpolarized mr. *NMR in Biomedicine*, 27:656–662, 2014.
- [8] Emeric Miclet, Daniel Abergel, Aurélien Bornet, Jonas Milani, Sami Jannin, and Geoffrey Bodenhausen. Toward quantitative measurements of enzyme kinetics by dissolution dynamic nuclear polarization. *The Journal of Physical Chemistry Letters*, 5(19):3290–3295, 2014. PMID: 26278433.
- [9] Aude Sadet, Emmanuelle M. M. Weber, Aditya Jhajharia, Dennis Kurzbach, Geoffrey Bodenhausen, Emeric Miclet, and Daniel Abergel. Rates of chemical reactions embedded in a metabolic network by dissolution dynamic nuclear polarisation nmr. *Chemistry A European Journal*, 24:5456–5461, 2018.
- [10] Talia Harris, Galit Eliyahu, Lucio Frydman, and Hadassa Degani. Kinetics of hyperpolarized ^{13}C -pyruvate transport and metabolism in living human breast cancer cells. *Proc Natl Acad Sci U S A*, 106:18131–6, 2009.
- [11] Talia Harris, Hadassa Degani, and Lucio Frydman. Hyperpolarized ^{13}C nmr studies of glucose metabolism in living breast cancer cell cultures. *NMR in Biomedicine*, 26:1831–1843, 2013.
- [12] Dmitry Shishmarev, Philip W. Kuchel, Guilhem Pagès, Alan J. Wright, Richard L. Hesketh, Felix Kreis, and Kevin M. Brindle. Glyoxalase activity in human erythrocytes and mouse lymphoma, liver and brain probed with hyperpolarized ^{13}C -methylglyoxal. *Communications Biology*, 1:232, 2018.
- [13] François Kayser, Monique Biesemans, Rudolph Willem, Francine Malaisse-Lagae, and Willy J. Malaisse. Does phosphoglucoisomerase display anomeric specificity or selectivity towards alpha-d-glucose 6-phosphate? an assessment by two-dimensional phase-sensitive ^{31}P exchange spectroscopy (exsy) nmr. *Biochemical journal*, 295(Pt 2):607, 1993.
- [14] Margarita Salas, Eladio Vinuela, and Alberto Sols. Spontaneous and enzymatically catalyzed anomerization of glucose-6-phosphate and anomeric specificity of related enzymes. *Journal of Biological Chemistry*, 240:561–586, 1965.
- [15] David Keilin and Edward F. Hartree. Biological catalysis of mutarotation of glucose. *Biochemical Journal*, 50:341–348, 1952.
- [16] J. Martyn Bailey, Peter H. Fishman, and Peter G. Pentchev. Studies on mutarotases. ii. investigations of possible rate-limiting anomerizations in glucose metabolism. *Journal of Biological Chemistry*, 243:4827–4831, 1968.
- [17] Bernd Wurster and Benno Hess. Glucose-6-phosphate-1-epimerase from baker’s yeast. a new enzyme. *FEBS Letters*, 23:341–344, 1972.
- [18] Bernd Wurster and Benno Hess. Anomeric specificity of enzymes of d-glucose metabolism. *FEBS Letters*, 40:S112–S118, 1974.

- [19] Edwin M. Chance, Benno Hess, Theodor Plessner, and Bernd Wurster. Determination of the kinetic constants of glucose-6-phosphate 1-epimerase by non-linear optimization. *European Journal of Biochemistry*, 50:419–424, 1975.
- [20] Dmitry Shishmarev, Lucas Quiquempoix, Clément Q. Fontenelle, Bruno Linclau, and Philip W. Kuchel. Anomerisation of fluorinated sugars by mutarotase studied using 19f nmr two-dimensional exchange spectroscopy. *Australian Journal of Chemistry*, 73:117–128, 2020.
- [21] Marc Graille, Jean-Pierre Baltaze, Nicolas Leulliot, Dominique Liger, Sophie Quevillon-Cheruel, and Herman van Tilbeurgh. Structure-based functional annotation - yeast ymr099c codes for a d-hexose-6-phosphate mutarotase. *The Journal of Biological Chemistry*, 281:30175–30185, 2006.
- [22] J. Martyn Bailey, Peter H. Fishman, and Peter G. Pentchev. Anomalous mutarotation of glucose 6-phosphate. an example of intramolecular catalysis. *Biochemistry*, 9:1189–1194, 1970.
- [23] Sivaranjan Uppala, Ayelet Gamliel, Gal Sapir, Jacob Sosna, J. Moshe Gomori, and Rachel Katz-Brull. Observation of glucose-6-phosphate anomeric exchange in real-time using ddnp hyperpolarised nmr. *Royal Society of Chemistry Advances*, 10:41197–41201, 2020.
- [24] Emeric Miclet, Véronique Stoven, Paul A. M. Michels, Frederic R. Opperdoes, Jean-Yves Lallemand, and Francis Duffieux. Nmr spectroscopic analysis of the first two steps of the pentose-phosphate pathway elucidates the role of 6-phosphogluconolactonase. *Journal of Biological Chemistry*, 276:34840–34846, 2001.
- [25] Aude Sadet. *Etudes de cinétiques enzymatiques par Polarisation Dynamique Nucléaire avec Dissolution (D-DNP) : application à l'étape oxydative de la voie des Pentoses Phosphates (PPP)*. PhD thesis, ENS - Paris, 2017.
- [26] Sami Jannin, Aurélien Bornet, Sonia Colombo, and Geoffrey Bodenhausen. Low-temperature cross polarization in view of enhancing dissolution dynamic nuclear polarization in nmr. *Chemical Physics Letters*, 517:234–236, 2011.
- [27] Guilhem Pagès, Max Puckeridge, Guo Liangfeng, Yee Ling Tan, Chacko Jacob, Marc Garland, and Philip W. Kuchel. Transmembrane exchange of hyperpolarized ^{13}C -urea in human erythrocytes: Subminute timescale kinetic analysis. *Biophysical Journal*, 105:1956–1966, 2013.
- [28] Philip W. Kuchel, Magnus Karlsson, Mathilde Hauge Lerche, Dmitry Shishmarev, and Jan Henrik Ardenkjær-Larsen. Rapid zero-trans kinetics of cs^+ exchange in human erythrocytes quantified by dissolution hyperpolarized ^{13}C nmr spectroscopy. *Scientific Reports*, 9:19726, 2019.
- [29] Athan J. Shaka, James H. Keeler, and Ray Freeman. Evaluation of a new broadband decoupling sequence: Waltz-16. *Journal of Magnetic Resonance*, 53:313–340, 1983.
- [30] William H. Press, Saul A. Teukolsky, William T. Vetterling, and Brian P. Flannery. *Numerical recipes, The Art of Scientific Computing, Third edition*. Cambridge University Press, 2007.
- [31] *Scilab, a free scientific software package*. Copyright 1989-2005. INRIA ENPC, www.scilab.org.
- [32] Rainer M. Storn and Kenneth V. Price. Differential evolution: A simple and efficient heuristic for global optimization over continuous spaces. *Journal of Global Optimization*, 11:341–359, 1997.
- [33] Kenneth V. Price, Rainer M. Storn, and Jouni A. Lampinen. *Differential Evolution - A Practical Approach to Global Optimization*. Studies in Computational Intelligence. Springer-Verlag Berlin Heidelberg, 2005.
- [34] Uday K. Chakraborty, editor. *Advances in Differential Evolution*. Studies in Computational Intelligence. Springer Berlin, Heidelberg, 2008.

- [35] Alan G. Marshall and Francis R. Verdun. *Fourier Transforms in Nmr, Optical, and Mass Spectrometry: A Users Handbook*. Elsevier Science Ltd, 1990.
- [36] Richard R. Ernst, Geoffrey Bodenhausen, and Alexander Wokaun. *Principles of Nuclear Magnetic Resonance in One and Two Dimensions*. Oxford Science Publications, 1990.
- [37] Christian Robert and George Casella. *Monte Carlo Statistical Methods*. Springer Texts in Statistics. Springer-Verlag, 2010.
- [38] Stuart J. Elliott, Quentin Stern, Morgan Ceillier, Théo El Daraï, Samuel F. Cousin, Olivier Cala, and Sami Jannin. Practical dissolution dynamic nuclear polarization. *Progress in Nuclear Magnetic Resonance Spectroscopy*, 126-127:59–100, 2021.
- [39] Arnab Dey, Benoît Charrier, Karine Lemaitre, Victor Ribay, Dmitry Eshchenko, Marc Schnell, Roberto Melzi, Quentin Stern, Samuel F. Cousin, James G. Kempf, Sami Jannin, Jean-Nicolas Dumez, and Patrick Giraudeau. Fine optimization of a dissolution dynamic nuclear polarization experimental setting for ^{13}C nmr of metabolic samples. *Magnetic Resonance*, 3(2):183–202, 2022.
- [40] Youngbok Lee, Gyu Seong Heo, Haifeng Zeng, Karen L. Wooley, and Christian Hilty. Detection of living anionic species in polymerization reactions using hyperpolarized nmr. *Journal of the American Chemical Society*, 135(12):4636–4639, 2013. PMID: 23461287.
- [41] C. Stan Tsai and Q. Chen. Purification and kinetic characterization of hexokinase and glucose-6-phosphate dehydrogenase from *Schizosaccharomyces pombe*. *Biochemistry and Cell Biology*, 76(1):107–113, 1998.
- [42] Alejandro G. Marangoni. *Enzyme Kinetics - A Modern Approach*. John Wiley & Sons, 2003.
- [43] Philip W. Kuchel and Dmitry Shishmarev. Dissolution dynamic nuclear polarization nmr studies of enzyme kinetics: Setting up differential equations for fitting to spectral time courses. *Journal of Magnetic Resonance Open*, 1:100001, 2019.
- [44] Karel Olavarria, Diego Valdés, and Ricardo Cabrera. The cofactor preference of glucose-6-phosphate dehydrogenase from *Escherichia coli* – modeling the physiological production of reduced cofactors. *the FEBS journal*, 279:2261–2466, 2012.
- [45] Karel Olavarria, Jessica De Ingeniis, D. C. Zielinsk, Matias Fuentealba, Rodrigo Muñoz, Bryan D. McCloskey, Adam M. Feist, and Ricardo Cabrera. Metabolic impact of an nadh-producing glucose-6-phosphate dehydrogenase in *Escherichia coli*. *Microbiology*, 160:2780–2793, 2014.
- [46] Matias Fuentealba, Rodrigo Muñoz, Pablo Maturana, Adriana Krapp, and Ricardo Cabrera. Determinants of cofactor specificity for the glucose-6-phosphate dehydrogenase from *Escherichia coli*: Simulation, kinetics and evolutionary studies. *PLOS One*, 11, 2016.

TOC figure

